Accepted Manuscript

This article can be cited before page numbers have been issued, to do this please use: L. Onel, R. Lade, J. Mortiboy, M. Blitz, P. Seakins, D. E. Heard and D. Stone, *Phys. Chem. Chem. Phys.*, 2021, DOI: 10.1039/D1CP02932K.

rsc.li/pccp

Kinetics of the Gas Phase Reaction of the Criegee Intermediate CH_2OO with SO_2 as a Function of Temperature

Lavinia Onel,[1] Rachel Lade,[1] Jennifer Mortiboy,[1] Mark Blitz,[1,2] Paul Seakins,[1] Dwayne

Heard,[1] and Daniel Stone[1*]

[1] School of Chemistry, University of Leeds, Leeds, LS2 9JT, UK

[2] National Centre for Atmospheric Science, University of Leeds, Leeds, LS2 9JT, UK

* Corresponding Author: d.stone@leeds.ac.uk, +44 113 343 6508

Abstract

The kinetics of the gas phase reaction of the Criegee intermediate CH_2OO with SO_2 have

been studied as a function of temperature in the range 223–344 K at 85 Torr using flash

photolysis of $CH_2I_2/O_2/SO_2/N_2$ mixtures at 248 nm coupled to time-resolved broadband UV

absorption spectroscopy. Measurements were performed under pseudo-first-order conditions

with respect to SO_2, revealing a negative temperature dependence. Analysis of experimental

results using the Master Equation Solver for Multi-Energy well Reactions (MESMER)

indicates that the observed temperature dependence, combined with the reported lack of a

pressure dependence in the range 1.5–760 Torr, can be described by a reaction mechanism

consisting of the formation of a pre-reaction complex leading to a cyclic secondary ozonide

which subsequently decomposes to produce $HCHO + SO_3$. The temperature dependence can

be characterised by $k_{CH2OO+SO2} = (3.72 \pm 0.13) \times 10^{-11} (T/298)^{(-2.05 \pm 0.38)}$ cm^3 molecule^{-1} s^{-1}.

The observed negative temperature dependence for the title reaction in conjunction with the

decrease in water dimer (the main competitor for the Criegee intermediate) concentration at

lower temperatures means that Criegee intermediate chemistry can play an enhanced role in

SO_2 oxidation in the atmosphere at lower temperatures.

Introduction

Criegee intermediates are reactive species produced in the atmosphere following the ozonolysis of unsaturated volatile organic compounds (VOCs) in environments impacted by biogenic and/or anthropogenic emissions.[1, 2] The exothermicity associated with ozonolysis reactions leads to the formation of nascent Criegee intermediates with high internal energy, which may undergo either unimolecular decomposition or collisional energy transfer with surrounding gas molecules to form stabilised Criegee intermediates (SCIs). Bimolecular reactions of stabilised Criegee intermediates with atmospheric constituents such as water vapour, water vapour dimers, NO_2, and SO_2 can impact atmospheric budgets of NO_x (NO + NO_2), SO_2 and H_2SO_4, sulfate aerosol, and secondary organic aerosol, and thus influence air quality and climate.[3-9] Welz et al.[4] reported the first direct measurements of SCI kinetics using the photolysis of CH_2I_2 at 248 nm in the presence of O_2 at low pressure (4 Torr) to generate the CH_2OO Criegee intermediate (R1-R2), coupled with tunable VUV synchrotron photoionization mass spectrometry (PIMS) to probe CH_2OO:

$$CH_2I_2 + h\nu \rightarrow CH_2I + I \qquad\qquad (R1)$$

$$CH_2I + O_2 \rightarrow CH_2OO + I \qquad\qquad (R2)$$

Welz et al. reported a rate coefficient of $(3.9 \pm 0.7) \times 10^{-11}$ cm^3 molecule^{-1} s^{-1} for the reaction of CH_2OO with SO_2 at 298 K in 4 Torr of He, which is several orders of magnitude larger than previous estimates based on indirect measurements in ozonolysis reactions, with potentially significant impacts on our understanding of SO_2 oxidation in the atmosphere.[1]

$$CH_2OO + SO_2 \rightarrow HCHO + SO_3 \qquad (R3)$$

Following the work of Welz et al., a number of studies investigating the kinetics of R3 have been performed at room temperature using the same photochemical source of CH_2OO (i.e. photolysis of CH_2I_2/O_2) but with different spectroscopic techniques used to detect either CH_2OO, [9-14] HCHO formed by reaction R3,[11] or OH as a proxy for CH_2OO.[15, 16] A summary of previous measurements of k_3, and techniques employed, is given in Table 1. The pressure dependence of the reaction was investigated by Stone et al.[11], with a pressure independent rate coefficient of $k_3 = (3.42 \pm 0.42) \times 10^{-11}$ cm^3 molecule^{-1} s^{-1} reported over the pressure range 1.5–450 Torr. The good agreement between the results of all the photolytic experiments (Table 1) suggest that the rate coefficient k_3 at room temperature is relatively well-characterised and shows no significant pressure dependence in the range 1.5 to 760 Torr.[17] The current IUPAC recommendations suggest a pressure independent rate coefficient of $k_3 = \left(3.70 \, ^{+0.45}_{-0.40}\right) \times 10^{-11}$ cm^3 molecule^{-1} s^{-1} at 298 K.[17] However, the temperature dependence of the $CH_2OO + SO_2$ reaction has yet to be reported, with such an investigation necessary to improve the understanding of the mechanism and atmospheric impacts of the reaction between CH_2OO and SO_2.

Reference	Technique	Photolysis	Temperature	Pressure/Torr	Bath	k_3/10^{-11} cm^3

		wavelength/nm	/K		gas	molecule^{-1} s^{-1}
Welz et al. 2012[4]	LFP[a]/PIMS[b]	248	298	4	He	3.9 ± 0.7
Sheps 2013[10]	LFP/UV abs[c]	266	295	5	He	4.1 ± 0.3
Stone et al. 2014[11]	LFP/LIF[d] HCHO	355	295	50–450	N$_2$	3.42 ± 0.42
	LFP/PIMS	248	295	1.5	He	
Liu et al. 2014[15]	LFP/LIF OH	351	295	50–200	Ar	3.53 ± 0.29
Chhantyal-Pun et al. 2015[12]	LFP/CRDS[e]	355	295	30	N$_2$	3.80 ± 0.04
Huang et al. 2015[13]	LFP/UV abs	248	298	30–756	N$_2$	3.57 ± 0.28
Liu et al. 2017[16]	LFP/LIF OH	355	300	10	Ar	3.88 ± 0.13
Howes et al. 2019[9]	LFP/PIMS	248	295	2	He	3.74 ± 0.43

	LFP/UV abs	248	295	50	N$_2$	3.87± 0.45
Qiu and Tonokura[14] 2019	LFP/mid-IR abs	266	295	10.4	N$_2$	3.6 ± 0.1

Table 1. Values for k_3 determined in photolytic experiments using a range of experimental techniques. [a] LFP = laser flash photolysis of CH$_2$I$_2$ in the presence of O$_2$. [b] PIMS = photoionisation mass spectrometry monitoring CH$_2$OO. [c] UV absorption = time-resolved broadband ultraviolet absorption spectroscopy. [d] LIF = laser induced fluorescence. [e] CRDS = cavity ring down spectroscopy.

Experimental studies employing LIF detection of HCHO produced in R3[11] suggest that HCHO and thus SO$_3$ are products of the reaction R3, with the co-product SO$_3$ directly observed by PIMS[18] at 4 Torr and transient infrared absorption spectroscopy at 110 and 214 Torr.[19] Theoretical studies also indicate that HCHO and SO$_3$ are the dominant products under atmospheric conditions, formed via a five-membered secondary ozonide (SOZ) cycloadduct[5, 20-22] and thus the SO$_2$-catalysed isomerisation of CH$_2$OO to formic acid via SOZ evidenced by Aplincourt and Rui-López[23] is a minor channel of the CH$_2$OO + SO$_2$ reaction. Experimental studies using PIMS[18] and transient infrared absorption spectroscopy[19] have not observed the reaction channel producing formic acid, also indicating that this channel is negligible. Vereecken et al.[5] and Kuwata et al.[22] have investigated the potential energy surface for the reaction between CH$_2$OO and SO$_2$, combined with Rice-Ramsperger-Kassel-Marcus (RRKM)/master equation simulations to predict product yields, but with contrasting results. Kuwata et al.[22] predicted a yield for HCHO + SO$_3$ of at least 97 % at atmospheric pressure, while Vereecken et al.[5] predicted a yield of 68 % HCHO + SO$_3$ at atmospheric pressure. Both studies report that the reaction is under the low-pressure regime, with

negligible stabilisation of the SOZ up to pressures considerably above ambient conditions.[5,22] However, the mechanisms for formation of the SOZ and for the subsequent production of HCHO and SO_3 differ in the two theoretical studies. Vereecken et al.[5] predicted barrierless formation of the SOZ in the initial $CH_2OO + SO_2$ encounter, with homolytic cleavage of the O–O bond in the SOZ yielding the biradical $OCH_2OS(O)O$, which in turn predominantly leads to HCHO and SO_3 by β-scission. The formation of formyl sulfinic acid, $HC(=O)OS(=O)OH$ (15% at 1 atm) and bisoxy diradical, $H_2C(O^\bullet)O^\bullet$, $+ SO_2$ (17% at 1 atm) by the decomposition of $OCH_2OS(O)O$ was also expected by Vereecken et al.[5] In contrast, Kuwata et al.[22] characterised the barrierless formation of a pre-reaction complex in the first reaction step, which then leads to the SOZ, with the reaction predominantly following a closed-shell pathway involving the direct formation of HCHO + SO_3 from the SOZ by cycloreversion, in qualitative agreement with the earlier studies of Jiang et al.[20] and Kurtén et al.[21] Kuwata et al.[22] employed a complex description of the potential energy surface, incorporating two distinct stereochemical pathways owing to the existence of diastereomeric *endo* and *exo* conformers of the SOZ. By combining the quantum chemical calculations with statistical rate theory models Kuwata et al.[22] predicted that $k_3 = (3.68 \pm 0.02) \times 10^{-11}$ cm^3 $molecule^{-1}$ s^{-1} at 295 K with no statistically significant variation with pressure between 1–760 Torr, in good agreement with the results of the photolytic experiments.

The formation of SO_3 by reaction R3 indicates that the reaction is potentially significant in the production of H_2SO_4 and sulfate aerosol in the atmosphere. Atmospheric modelling studies have shown that a larger rate coefficient for $CH_2OO + SO_2$ has a significant impact on sulfate aerosol formation on regional scale[6] and on gas phase H_2SO_4 production in forested regions such as a boreal forest in Finland[24] and tropical forests.[25] However, the modelling

results do depend on the competition between the reaction of CH_2OO with SO_2 and that with water vapour/water vapour dimers, with a number of recent studies indicating that the reaction of CH_2OO with water dimers is more important than the CH_2OO + water monomer reaction under atmospheric relevant conditions.[26-29] IUPAC currently recommends a value of $(6.4 \pm 1.5) \times 10^{-12}$ cm^3 molecule^{-1} s^{-1} for the rate coefficient of the CH_2OO + $(H_2O)_2$ reaction, which is four orders of magnitude larger than the rate coefficient of the CH_2OO + H_2O reaction, $(2.8 \pm 1.1) \times 10^{-16}$ cm^3 molecule^{-1} s^{-1}.[30] Kinetic studies of the CH_2OO + $(H_2O)_2$ reaction[30] have led to the conclusion that the removal of CH_2OO in the troposphere is dominated globally by the reaction with water dimer.[2] However, the reaction of CH_2OO with SO_2 is fast enough to potentially compete with the CH_2OO + water dimer reaction and impact on SO_2 oxidation in SO_2–rich environments and/or low absolute humidities. As the concentration of water dimer varies strongly with the saturated vapor pressure of water, the competition between SO_2 and water dimer for CH_2OO will be temperature dependent.

In the present work we report the kinetics of the CH_2OO + SO_2 reaction at 85 Torr in the temperature range of 223 – 344 K using 248 nm photolysis of $CH_2I_2/O_2/SO_2/N_2$ mixtures under pseudo-first-order conditions with respect to SO_2. Time-resolved broadband UV absorption spectroscopy was employed to monitor CH_2OO directly during the reaction with SO_2. This is the first study of the temperature dependence of the rate coefficient for the CH_2OO + SO_2 reaction.

Experimental

The kinetics of the CH_2OO + SO_2 reaction were studied as a function of temperature using laser flash photolysis of $CH_2I_2/O_2/SO_2/N_2$ gas mixtures, coupled with time-resolved

broadband UV absorption spectroscopy. The experimental apparatus has been described in detail previously[31-33] therefore only a brief description is given here.

Two reaction cells were used, both consisting of a 100 cm long glass tube of 3 cm inner diameter sealed with fused silica windows at both ends. The first cell was jacketed and used for experiments at $T \geq 296$ K, in which the temperature was controlled by circulating thermofluid (HUBE6479 DW-therm oil) from a thermoregulator (Huber Unistat 360). The second reaction cell, used for temperatures at $T < 296$ K, was immersed in a cooling bath of 30 % ethane-1,2-diol in methanol and surrounded by 3 cm thick polystyrene for insulation. The temperature for this cell was controlled using a refrigerated immersion chiller (LabPlant Refrigerated Immersion Probe, RP-100CD), with the probe immersed in the cooling mixture and magnetic stirring employed to achieve a constant temperature (within 98 %) in the cooling mixture along the cell. Further details of temperature calibrations in the cell are given in the Supplementary Information.

A dilute mixture of SO_2 (Sigma-Aldrich, 99.9%) was prepared manometrically at a known concentration in nitrogen (BOC 99.998 %) and stored in a glass bulb. Gases, i.e. SO_2, O_2 (BOC, 99.5 %) and the carrier gas N_2, were introduced through calibrated mass flow controllers (MFCs) in a glass mixing manifold. A few percent of the gas mixture was then passed through a bubbler containing liquid CH_2I_2 (Alfa Aesar, 99 %) held at constant temperature in an ice bath, which was then mixed with the remaining fraction of the gas and delivered to the reaction cell. The initial concentration of CH_2I_2 in the cell was controlled by a needle valve at the entrance of the bubbler and determined by UV absorption measurements as the average of the concentration in the cell before and after each kinetic run.

The kinetic experiments were performed under pseudo-first-order conditions with respect to SO_2. The initial concentrations were: $[SO_2] = (0.6 - 5.6) \times 10^{13}$ molecule cm^{-3} (typical uncertainties of $\sim$ 5 %), $[CH_2I_2] = (1.0 - 7.4) \times 10^{13}$ molecule cm^{-3}, $[O_2] = 7.5 \times 10^{17}$ molecule cm^{-3} and $[CH_2OO]_0 = (0.4 - 2.7) \times 10^{12}$ molecule cm^{-3}.

The total flow rate was 18 slm, giving a residence time in the cell of ~2 s. The total pressure in the cell was maintained at 85 Torr and measured by a capacitance manometer (MKS Instruments). The chemistry within the cell was initiated by pulsed excimer laser photolysis at 248 nm (KrF, Lambda-Physik CompEx 210) with a laser fluence of $2–6 \times 10^{16}$ photon cm^{-2} (measured by a Molectron Powermax 500A power meter). The pulse repetition rate was 0.3 Hz to ensure a fresh gas mixture in the cell for each laser pulse.

Absorption of UV/visible radiation during the experiments was monitored using a laser-driven light source (LDLS, Energetiq EQ-99X), which provides ~10 mW cm^{-2} of light between 200 nm and 800 nm. Approximately 10 % of the probe light was aligned in a single pass arrangement along the length of the cell, which was used in the temperature calibrations (see Supplementary Information) with the remaining light used for the kinetics measurements aligned in a 7 pass arrangement described previously.[31-33] The total effective pathlength in the multi-pass arrangement, considering the total overlap between the photolysis and probe beams, was determined to be $l = (471 \pm 50)$ cm from comparison between the expected depletion of $[CH_2I_2]$ owing to photolysis ($\Delta[CH_2I_2]$), based on the measured concentration of CH_2I_2 and laser fluence in the cell, and $\Delta[CH_2I_2] \times l$ derived from analysis of the post-photolysis absorption spectra. Further details are given in the Supplementary Information. It should be noted that the value obtained for the total pathlength did not impact the determination of the rate coefficient of the $CH_2OO + SO_2$ reaction as the kinetic experiments were performed under pseudo-first-order conditions.

The probe beam exiting the reaction cell was passed through a sharp cut-on filter (248 nm RazorEdge ultrasteep long-pass edge filter, Semrock) to minimise the impacts of scattered excimer light and focused onto a fibre optic via a fibre launcher (Elliot Scientific). The output

from the fibre optic was directed through a 25 μm slit onto a spectrograph equipped with a diffraction grating of 300 grooves/mm and imaged onto an integrated thermoelectrically cooled charge-coupled device (CCD) detector (FER-SCI-1024BRX, Princeton Instruments), giving spectral resolution of 1 nm (FWHM). The exposure time of the CCD to the light was varied from 10 – 100 μs. The spectral and temporal information were mapped spatially along the horizontal and vertical directions of the CCD, respectively, as described in detail in our previous work.[33] The photocharge was shifted on the time axis (vertically) from an illuminated region to a storage region with a programmable rate in the range 5.6 μs/row to 35 μs/row. The rapid shift of photocharge on the CCD resulted in an instrument response function, which was included in the analysis of the measured concentration-time profiles as described in the Results section.

Wavelength calibrations were performed by recording the well-known Hg emission spectrum from a low pressure Hg pen-ray lamp (Oriel). Timings of the recording by the camera and the firing of the photolysis laser were controlled by a delay generator (SRS DG535). Intensity data recorded by the camera were typically averaged for 400–800 photolysis shots and transferred to a PC for analysis.

Results

Figure 1 shows an example of total absorbance recorded following photolysis, with contributions from the absorbance of CH_2I_2, CH_2OO and IO. The absorbance, $A(\text{tot})_{\lambda,t}$, was

observed as a function of wavelength (λ) and time (t) and analysed between 300 and 450 nm to determine the changes to concentrations of each species by fitting the reference absorption cross-sections for CH_2OO,[32] IO[34] and CH_2I_2[35] to $A(\text{tot})_{\lambda,t}$ at each time point (E1).

$$A(\text{tot})_{\lambda,t} = \ln\left(\frac{I^{\lambda,0}}{I^{\lambda,t}}\right) = \sum_i \sigma^{i,\lambda} \cdot [i]_t \cdot l \qquad \text{(E1)}$$

where $I_{\lambda,0}$ is the average light intensity at wavelength λ prior to photolysis, $I_{\lambda,t}$ is the post-photolysis intensity at wavelength λ and time t, $\sigma_{i,\lambda}$ is the cross section of species i at wavelength λ, $[i]_t$ is the concentration of species i at time t, and l is the total pathlength, (471 ± 50) cm.
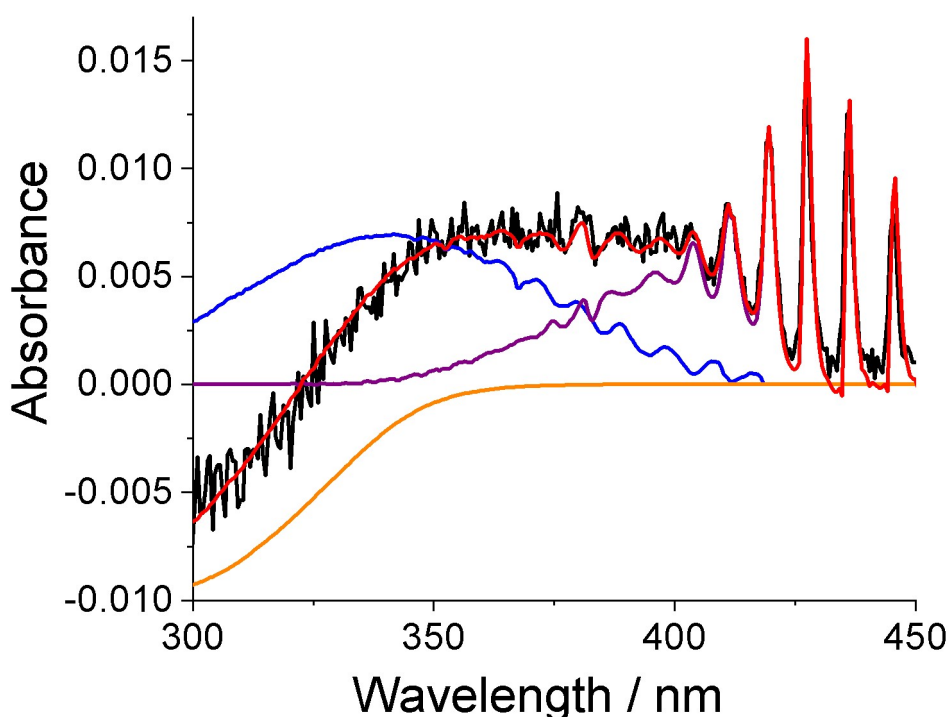

Figure 1. Observed absorbance (black), total fit (red), and the individual contributions from CH_2OO (blue), IO (purple) and CH_2I_2 (orange) determined by fitting reference spectra to the measured absorbance using eq E1 at $t = 1.0$ ms following photolysis. For these data, $T = 296$

K, p = 85 Torr, $[O_2]$ = 7.5 × 10^{17} molecule cm^{-3}, $[CH_2I_2]$ = 8.0 × 10^{13} molecule cm^{-3}, $[CH_2OO]_0$ = 1.8 × 10^{12} molecule cm^{-3} and $[SO_2]$ = 5.0 × 10^{12} molecule cm^{-3}.

Figure 2 shows typical concentration–time profiles for CH_2OO, which are given by a convolution of the 'true' kinetic decay with an instrument response function (IRF).[33] The IRF is generated by the shift of the photocharge in the time direction of the CCD detector from the illuminated region to the storage region of the CCD (details in the Experimental). The rate coefficient for $CH_2I + O_2$ (1.1 × 10^{-12} cm^3 $molecule^{-1}$ s^{-1})[36] and the O_2 concentration (7.5 × 10^{17} molecule cm^{-3}) employed in this work indicate a time scale of 1 – 2 μs for the CH_2OO growth following photolysis. However, owing to the IRF, the observed $[CH_2OO]$ increases on a time scale of hundreds of μs before the subsequent decay which occurs on a time scale of 5 – 10 ms (Figure 2). Typical concentration-time profiles for CH_2I_2 and IO are given in the Supplementary Information.

As the kinetic experiments were performed under pseudo-first-order conditions with respect to SO_2 the decay of $[CH_2OO]$ by reaction with SO_2 (R3) is described by an exponential decay (E2).

$$[CH_2OO]_t = [CH_2OO]_0 \exp(- k_{obs} t) \qquad (E2)$$

Here $[CH_2OO]_t$ is the concentration of CH_2OO at time t, $[CH_2OO]_0$ is the concentration at time zero and k_{obs} is the observed rate coefficient. The parameter k_{obs} includes contributions from both the decay rate coefficient of CH_2OO in the absence of SO_2, k_{loss} and the pseudo-first-order rate coefficient for the reaction of CH_2OO with SO_2, which is given by the product of the bimolecular rate coefficient for the $CH_2OO + SO_2$ reaction, k_3 and $[SO_2]$ (E3).

$$k_{obs} = k_{loss} + k_3[SO_2] \qquad (E3)$$

where k_{loss} includes contributions from the first-order coefficient for the loss of CH_2OO by diffusion out of the probe region, the bimolecular rate coefficient for the CH_2OO self-reaction and the bimolecular rate coefficients for the reactions of CH_2OO with other reactive species generated in the CH_2I_2/O_2 photolytic mixture, predominately the reaction of CH_2OO with iodine atoms.[32]

The observed temporal behaviour of CH_2OO can be described by a convolution of the exponential decay described by equation E2 with the IRF described by a Gaussian centred at time t_c with width w (E4).[33]

$$[CH_2OO]_t = \frac{[CH_2OO]_0}{2} \exp\left[\frac{(k_{obs}w)^2}{2} - k_{obs}(t - t_c)\right]\left[1 + \mathrm{erf}\left(\frac{t - t_c - k_{obs}w^2}{\sqrt{2}w}\right)\right] \qquad (E4)$$

where erf is the error function encountered in integrating the normal distribution (the normalised form of the Gaussian function).[37]

Equation E4 was employed in the fit to the observed temporal profiles of CH_2OO at each temperature to determine k_{obs} and the Gaussian parameters t_c and w. The parameters t_c and w are dependent on the exposure time of the CCD detector to the light and the shift rate of the photocharge from the illuminated region to the storage region of the CCD. Concentration-time profiles obtained using the same exposure time and shift rate were fitted globally to determine the parameters t_c and w. Figure 2 shows an example of the global fit.
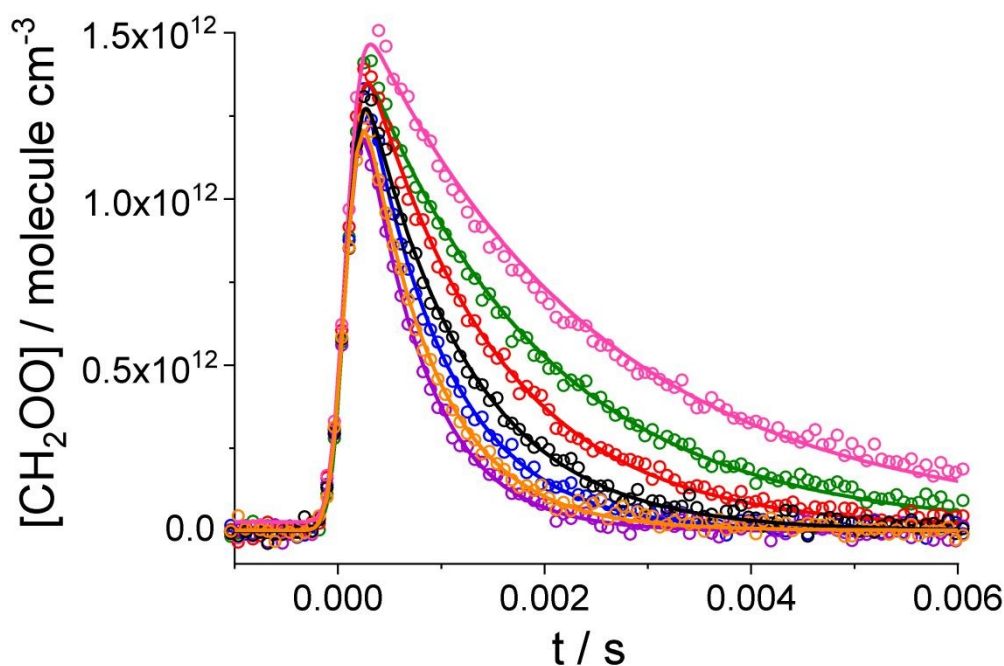
Figure 2. Examples of observations of CH_2OO (open circles) and fit results (solid lines). For this experiment $T = 316$ K and $p = 85$ Torr. The initial concentration of the precursor was the same for all the kinetic decays, $[CH_2I_2]_0 = 4.2 \times 10^{13}$ molecule cm^{-3}, while the initial concentration of SO_2 was varied from one measurement to another: no SO_2 (pink circles), 0.5×10^{13} molecule cm^{-3} (green circles), 0.9×10^{13} molecule cm^{-3} (red circles), 1.5×10^{13} molecule cm^{-3} (black circles), 2.0×10^{13} molecule cm^{-3} (blue circles), 2.6×10^{13} (orange circles) and 3.1×10^{13} (purple circles). The global fit to the data using equation E4 results in the observed rate coefficients for the CH_2OO reaction with SO_2, k_{obs}: 435 ± 5 (pink), 571 ± 5 s^{-1} (green), 783 ± 7 s^{-1} (red), 1002 ± 11 s^{-1} (black), 1261 ± 15 s^{-1} (blue), 1460 ± 19 s^{-1} (orange) and 1658 ± 23 s^{-1} (purple). For these data the IRF parameters are $t_c = (7.0 \pm 0.1) \times 10^{-5}$ s and $w = (1.20 \pm 0.02) \times 10^{-4}$ s. Errors are given at 1σ level.

Under given conditions the decay rate coefficient of CH_2OO in the absence of SO_2, k_{loss} is constant, hence a plot of k_{obs} as a function of $[SO_2]$ is linear with gradient k_3 (equation E3). Typical k_{obs} vs. $[SO_2]$ plots are shown in Figure 3 at four different temperatures: 223 K, 270 K, 296 K and 344 K. It can be observed that k_3 decreases with temperature. The plots of k_{obs} against $[SO_2]$ at all temperatures employed are shown in the Supplementary Information. The

values of k_3 determined at all temperatures are shown in Table 2. The temperature
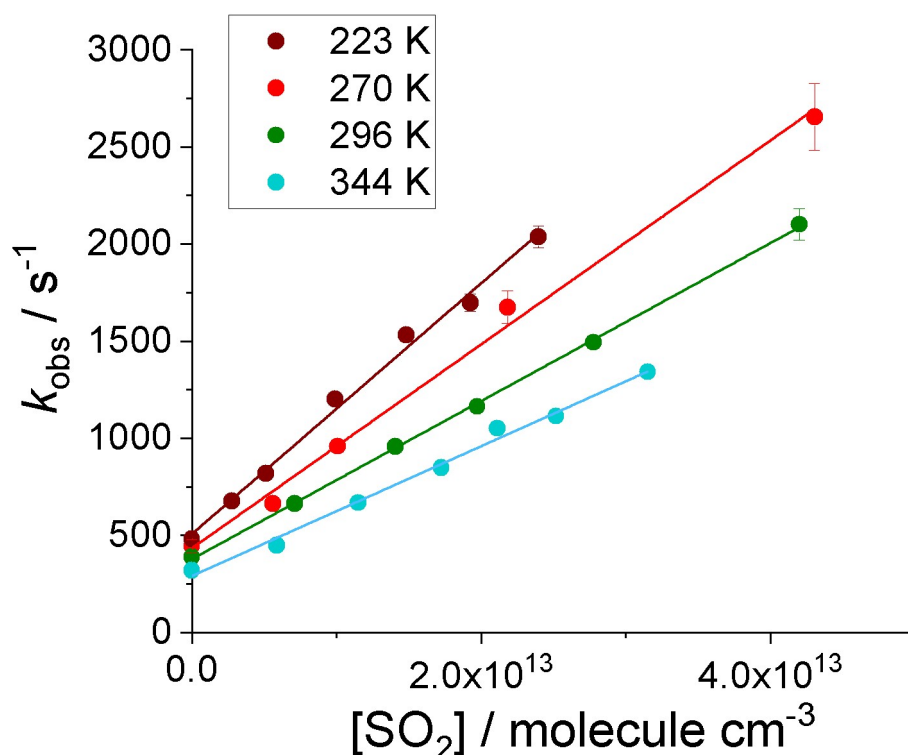
dependence of k_3 is shown in Figure 4.

Figure 3. k_{obs} vs. [SO$_2$] plots at 85 Torr and four different temperatures. The linear fits to the data result in the second order rate coefficients k_3 for each temperature: $(6.4 \pm 0.3) \times 10^{-11}$ cm^3 molecule^{-1} s^{-1} (223 K, dark red), $(5.3 \pm 0.3) \times 10^{-11}$ cm^3 molecule^{-1} s^{-1} (270 K, red), $(4.0 \pm 0.1) \times 10^{-11}$ cm^3 molecule^{-1} s^{-1} (296 K, green) and $(3.3 \pm 0.1) \times 10^{-11}$ cm^3 molecule^{-1} s^{-1} (344 K, blue). For each temperature [CH$_2$I$_2$] was constant: 3.4×10^{13} molecule cm^{-3} (dark red), 5.0×10^{13} molecule cm^{-3} (red), 4.8×10^{13} molecule cm^{-3} (green) and 4.5×10^{13} molecule cm^{-3} (blue). Laser fluence: 6.0×10^{16} photons cm^{-2} (dark red), 4.0×10^{16} photons cm^{-2} (red), 4.0×10^{16} photons cm^{-2} (green) and 3.0×10^{16} photons cm^{-2} (blue). Intercepts of the bimolecular plots are noted to decrease with increasing temperature, and are expected to be dominated by the reactions CH$_2$OO + CH$_2$OO and CH$_2$OO + I.[32] The rates of these reactions are expected to decrease with increasing temperature and are lower at the lower initial CH$_2$OO and I concentrations at higher temperatures owing to lower laser fluence used in experiments at higher temperatures.

Temperature/K	$k_3/10^{-11}$ cm^3 molecule^{-1} s^{-1}
223	6.4 ± 0.3
259	5.5 ± 0.3
266	4.4 ± 0.3
270	5.3 ± 0.3
275	4.1 ± 0.5
281	4.1 ± 0.1
296	4.0 ± 0.1
316	4.2 ± 0.1
324	3.6 ± 0.2
331	3.4 ± 0.1
340	2.2 ± 0.1

344	3.3 ± 0.1

Table 2. Values for k_3 determined in this work at $p = 85$ Torr and different temperatures.

Master equation calculations for the temperature dependence of the CH$_2$OO + SO$_2$ reaction using the MESMER program

A master equation analysis using the Master Equation Solver for Multi-Energy well Reactions (MESMER) was used to fit the potential energy surface (PES) for R3 to the experimental rate coefficients. A full description of MESMER is given in previous work.[38-41] MESMER solves the master equation and the subsequent eigenvalue–eigenvector analysis outputs the time profiles of species concentrations together with the phenomenological rate coefficients for the system. The most recent computational study of the CH$_2$OO + SO$_2$ by Kuwata et al.[22] expanded the understanding of the reaction mechanism by characterising two distinct stereochemical pathways to provide a detailed description of the PES. The authors[22] predicted that ~90 − 91% of the reaction proceeds through a closed-shell transition structure to form HCHO + SO$_3$, in qualitative agreement with previous studies,[20, 21] with a small contribution (6 − 7 %) of the open-shell mechanism leading to HCHO + SO$_3$ predicted by Vereecken et al. to be the dominant channel.[5] The present calculations were based on a potential energy surface shown in Figure 5, which was obtained by reducing the PES determined by Kuwata et al.[22] to the dominant closed-shell mechanism. The reaction first proceeds by the formation of a pre-reaction complex leading to a cyclic secondary ozonide (SOZ). The SOZ subsequently decomposes, producing HCHO + SO$_3$ via two stereochemical pathways arising from the existence of *endo* and *exo* conformers of the pre-reaction complex (species 3a and 3b respectively in Figure 5, using the same notation of the structures given by Kuwata et al.[22]) and of the SOZ (species 5a and 5b in Figure 5). Simulations using MESMER showed that there was no significant loss of accuracy by the reduction in complexity of the PES to that shown in Figure 5, and that the reduced mechanism dominates the fate of the CH$_2$OO + SO$_2$ under all conditions used in the MESMER calculations ($T = 223 − 344$ K and $p = 2 − 760$ Torr).

To characterise the observed negative temperature dependence and the pressure independence in the range $1.5 − 760$ Torr[11, 13] of the CH$_2$OO + SO$_2$ reaction, the values of k_3 obtained in this

17

work for $T = 220 - 350$ K and $p = 85$ Torr and the 298 K IUPAC recommendation for $p = 2$

760 Torr, k_3(298K, IUPAC) $= \left(3.70\,{}^{+0.45}_{-0.40}\right) \times 10^{-11}$ cm^3 molecule^{-1} s^{-1},[30] were fitted in

MESMER. The inverse Laplace transform (ILT) method was used to describe the barrierless

formation of the pre-reaction complexes 3a and 3b, giving a canonical high pressure limiting

rate coefficient $k^\infty = (5.5 \pm 2.0) \times 10^{-11}$ $(T/298)^{-(1.0 \pm 0.4)}$ for each stereo-chemical pathway. The

calculations showed that the cycloaddition transition states TS-4a and TS-4b control the

reaction rate and thus the relative energies of TS-4a and TS-4b were floated during the

simulations. The energies of the pre-reaction complexes 3a and 3b and the transition states

TS-4a and TS-4b were linked[42] to maintain the same relative differences as those given by

Kuwata et al.[22] The values calculated by Kuwata et al.[22] were used for the relative energies of

5a, 5b, TS-7a, TS-7b and the products HCHO and SO$_3$. The fit results for k_3 can be

parameterised by $k_3 = (3.72 \pm 0.13) \times 10^{-11}$ $(T/298)^{(-2.05 \pm 0.38)}$ cm^3 molecule^{-1} s^{-1} and are shown

in Figure 4. The fit values for the energies of 3a, 3b, TS-4a and TS-4b (relative to CH$_2$OO +

SO$_2$) are shown in Figure 5, which also shows the values calculated by Kuwata et al.[22] An

agreement within 98 % was obtained between the fit energies for 3a, 3b, TS-4a and TS-4b

determined by MESMER and the energies predicted by Kuwata et al.[22], i.e. the energies

given by MESMER calculations are 0.9 kJ mol^{-1} more negative than the values of Kuwata et

al. (Figure 5). This small deviation is within the 2.5 kJ mol^{-1} errors of the MESMER

calculations and the errors generated using the multi-coefficient Gaussian-3 quantum

chemical method (MCG3) employed by Kuwata et al.[22] to determine the energies of 3a, 3b,

TS-4a and TS-4b (root-mean-squared error of 6.6 kJ mol^{-1}).[43]
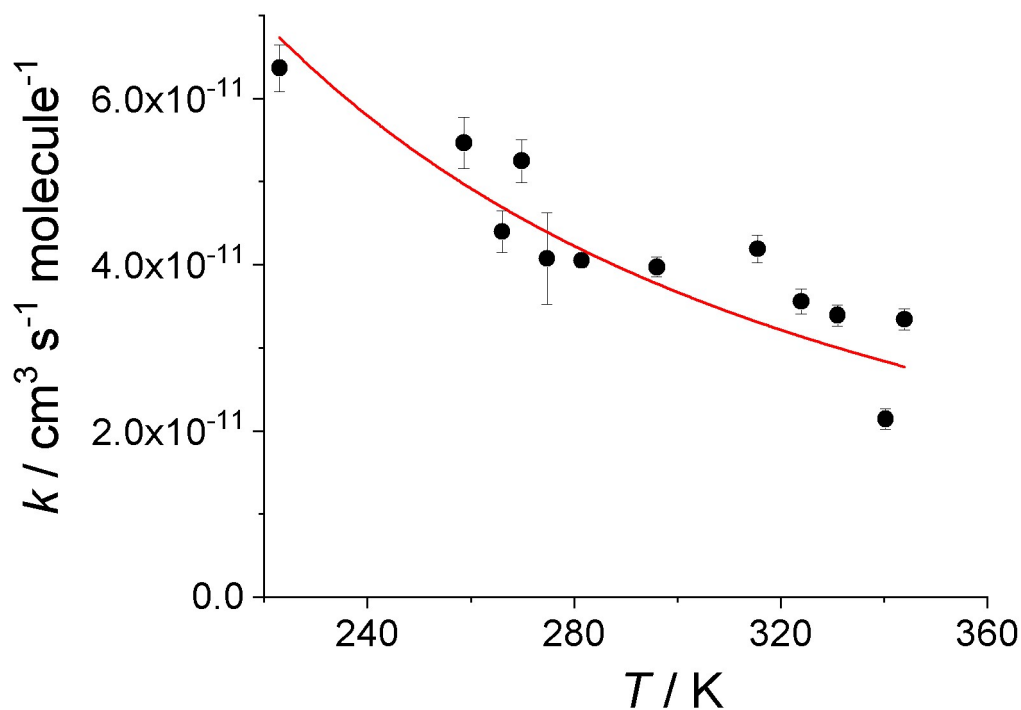
Figure 4. Temperature dependence of the rate coefficient for the $CH_2OO + SO_2$ reaction. The data are shown as black circles; error margins are statistical errors at 1σ level. The red line shows the parameterisation of the MESMER result, which gave $k_3 = (3.72 \pm 0.13) \times 10^{-11}$ $(T/298)^{(-2.05 \pm 0.38)}$ cm^3 molecule^{-1} s^{-1}.
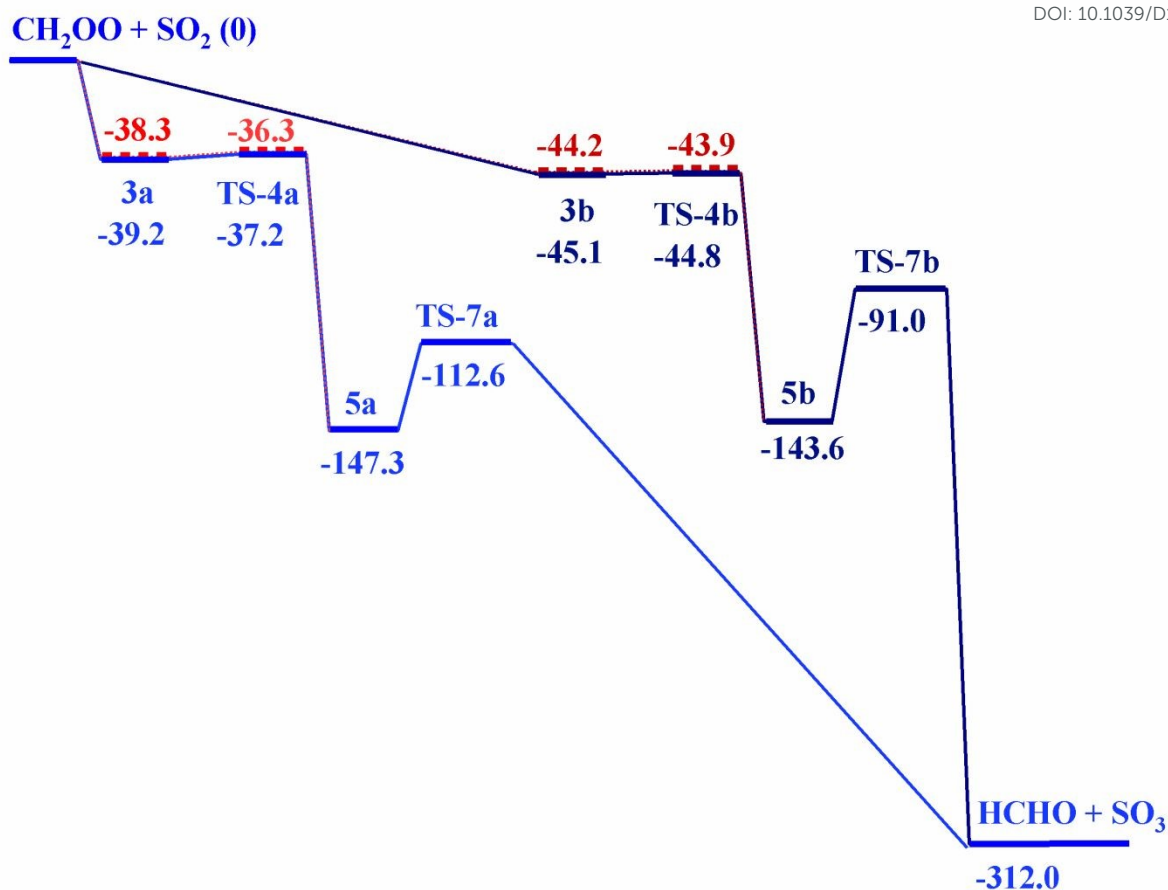
Figure 5. Potential energy surface of the reaction $CH_2OO + SO_2$ showing the two stereochemical pathways proceeding through *endo* (light blue) and *exo* conformers (dark blue). Energies (kJ mol^{-1}) of 3a, 3b, TS-4a and TS-4b were generated by MESMER calculations, while the energies of 5a, 5b, TS-7a, TS-7b and the products HCHO and SO$_3$ were taken from the work of Kuwata et al.[22] The energy levels calculated by Kuwata et al.[22] for 3a and TS-4a are shown in light red and for 3b and TS-4b are shown in dark red. The notations for intermediates and transitions states are the same as in the work of Kuwata et al.[19, 22] Kuwata et al. describe the structures of the species.[22]

A negative temperature dependence has also been observed for the reaction of the Criegee intermediate $(CH_3)_2COO$ with SO_2 between 283 and 303 K at 300 Torr following photolysis of $(CH_3)_2CI_2/O_2/N_2/SO_2$ mixtures at 248 nm coupled with time-resolved UV absorption at 340 nm. [44] The kinetics of the reaction were characterised by $k_{(CH3)2COO+SO2} = (1.36 \pm 0.03) \times 10^{-11} (T/298)^{(-6.45 \pm 0.64)}$ cm^3 molecule^{-1} s^{-1}, and the dependence on temperature is thus more pronounced than that observed for $CH_2OO + SO_2$ in the current study, $k_{CH2OO+SO2} = (3.72 \pm 0.13) \times 10^{-11} (T/298)^{(-2.05 \pm 0.38)}$ cm^3 molecule^{-1} s^{-1}.

Atmospheric Implications

Figure 6 compares the pseudo-first-order losses of CH_2OO for a range of SO_2 mixing ratios and relative humidities as a function of temperature. Losses to SO_2 are given as $k_3[SO_2]$, using the results for k_3 determined in this work. Losses as a function of relative humidity are given as the product of the current IUPAC recommendation for the temperature dependence of the reaction between CH_2OO and $(H_2O)_2$[17, 28] and the water dimer concentration, which was determined from the saturated vapour pressure of water[45], relative humidity, and the equilibrium constant for $2\ H_2O \rightleftharpoons (H_2O)_2$.[28, 46] Although the reaction with water dimers dominates under most conditions, the reaction of CH_2OO with SO_2 is potentially important in regions with high SO_2 concentrations and low humidity, particularly at low temperatures. Results for k_3 obtained in this work may be useful for the interpretation of field measurements and data obtained in chamber experiments at temperatures away from 298 K.
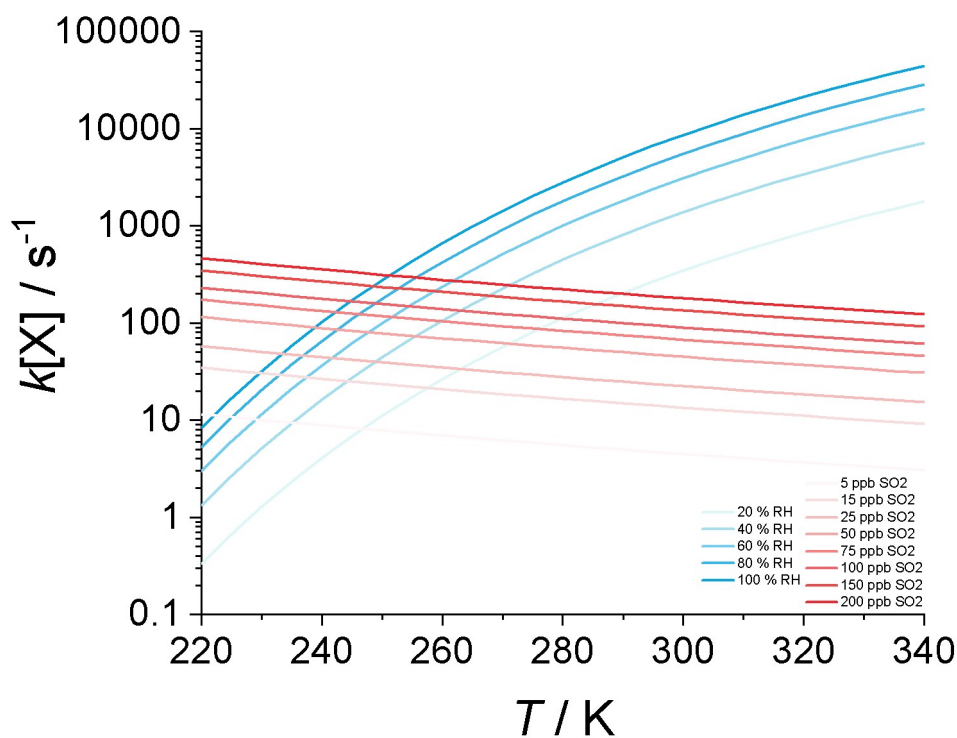
Figure 6. Comparison of pseudo-first-order losses for CH_2OO for a range of SO_2 mixing ratios and relative humidities as a function of temperature. Losses for CH_2OO are shown as $k[X]$, where X is SO_2 or $(H_2O)_2$, and have been determined using results obtained in this work for $k(T)[SO_2]$, with $k(T)[(H_2O)_2]$ determined from current IUPAC recommendations[17] for $CH_2OO + (H_2O)_2$ kinetics and water dimer concentrations determined from the saturated vapour pressure for water,[45] relative humidity, and the equilibrium constant for $2\ H_2O \rightleftharpoons (H_2O)_2$.[28, 46]

Conclusions

The kinetics for the reaction between the stabilised Criegee intermediate CH_2OO and SO_2 have been determined as a function of temperature using laser flash photolysis of $CH_2I_2/O_2/SO_2/N_2$ mixtures at 248 nm coupled to time-resolved broadband UV absorption spectroscopy in the temperature range 223 – 344 K at a total pressure of 85 Torr. The reaction showed a negative temperature dependence which can be described by $k_3 = (3.72 \pm 0.13) \times 10^{-11}\ (T/298)^{(-2.05 \pm 0.38)}$ cm^3 molecule^{-1} s^{-1}.

Calculations in MESMER[38] using a mechanism based on that proposed by Kuwata et al.[22] show that the measured negative temperature dependence and the lack of pressure dependence between 1.5 – 760 Torr[11, 13, 30] can be described by the barrierless formation of *endo* and *exo* pre-reaction complexes, which lead to *endo* and *exo* secondary cyclic ozonides through relatively low barriers. The secondary ozonides further decompose to $HCHO + SO_3$. The energies of the transition states leading from the pre-reaction complexes to the SOZs were found to be 0.9 kJ mol^{-1} more negative than those reported in the computational study of Kuwata et al.[22] In addition, this work reinforces the prediction of these authors that the reaction yield of $HCHO + SO_3$ at atmospheric pressure is close to 100 % and is in agreement with experimental work[19] finding that $HCHO + SO_3$ are the major products of the reaction.

Acknowledgements

References

1. Johnson, D.; Marston, G., The gas-phase ozonolysis of unsaturated volatile organic compounds in the troposphere. *Chemical Society Reviews* **2008,** *37* (4), 699-716.

2. Taatjes, C. A., Criegee Intermediates: What Direct Production and Detection Can Teach Us About Reactions of Carbonyl Oxides. In *Annual Review of Physical Chemistry, Vol 68*, Johnson, M. A.; Martinez, T. J., Eds. 2017; Vol. 68, pp 183-207.

3. Vereecken, L., Lifting the Veil on an Old Mystery. *Science* **2013,** *340* (6129), 154-155.

4. Welz, O.; Savee, J. D.; Osborn, D. L.; Vasu, S. S.; Percival, C. J.; Shallcross, D. E.; Taatjes, C. A., Direct Kinetic Measurements of Criegee Intermediate (CH_2OO) Formed by Reaction of CH_2I with O_2. *Science* **2012,** *335* (6065), 204-207.

5. Vereecken, L.; Harder, H.; Novelli, A., The reaction of Criegee intermediates with NO, RO_2, and SO_2, and their fate in the atmosphere. *Physical Chemistry Chemical Physics* **2012,** *14* (42), 14682-14695.

6. Percival, C. J.; Welz, O.; Eskola, A. J.; Savee, J. D.; Osborn, D. L.; Topping, D. O.; Lowe, D.; Utembe, S. R.; Bacak, A.; McFiggans, G.; Cooke, M. C.; Xiao, P.; Archibald, A. T.; Jenkin, M. E.; Derwent, R. G.; Riipinen, I.; Mok, D. W. K.; Lee, E. P. F.; Dyke, J. M.; Taatjes, C. A.; Shallcross, D. E., Regional and global impacts of Criegee intermediates on atmospheric sulphuric acid concentrations and first steps of aerosol formation. *Faraday Discussions* **2013,** *165*, 45-73.

7. Chhantyal-Pun, R.; Rotavera, B.; McGillen, M. R.; Khan, M. A. H.; Eskola, A. J.; Caravan, R. L.; Blacker, L.; Tew, D. P.; Osborn, D. L.; Percival, C. J.; Taatjes, C. A.; Shallcross, D. E.; Orr-Ewing, A. J., Criegee Intermediate Reactions with Carboxylic Acids: A Potential Source of Secondary Organic Aerosol in the Atmosphere. *Acs Earth and Space Chemistry* **2018,** *2* (8), 833-842.

8.   Khan, M. A. H.; Percival, C. J.; Caravan, R. L.; Taatjes, C. A.; Shallcross, D. E., Criegee intermediates and their impacts on the troposphere. *Environmental Science-Processes & Impacts* **2018,** *20* (3), 437-453.

9.   Howes, N. U. M.; Mir, Z. S.; Blitz, M. A.; Hardman, S.; Lewis, T. R.; Stone, D.; Seakins, P. W., Kinetic studies of C_1 and C_2 Criegee intermediates with SO_2 using laser flash photolysis coupled with photoionization mass spectrometry and time resolved UV absorption spectroscopy. *Physical Chemistry Chemical Physics* **2018,** *20* (34), 22218-22227.

10.   Sheps, L., Absolute Ultraviolet Absorption Spectrum of a Criegee Intermediate CH_2OO. *Journal of Physical Chemistry Letters* **2013,** *4* (24), 4201-4205.

11.   Stone, D.; Blitz, M.; Daubney, L.; Howes, N. U. M.; Seakins, P., Kinetics of CH_2OO reactions with SO_2, NO_2, NO, H_2O and CH_3CHO as a function of pressure. *Physical Chemistry Chemical Physics* **2014,** *16* (3), 1139-1149.

12.   Chhantyal-Pun, R.; Davey, A.; Shallcross, D. E.; Percival, C. J.; Orr-Ewing, A. J., A kinetic study of the CH_2OO Criegee intermediate self-reaction, reaction with SO_2 and unimolecular reaction using cavity ring-down spectroscopy. *Physical Chemistry Chemical Physics* **2015,** *17* (5), 3617-3626.

13.   Huang, H. L.; Chao, W.; Lin, J. J. M., Kinetics of a Criegee intermediate that would survive high humidity and may oxidize atmospheric SO_2. *Proceedings of the National Academy of Sciences of the United States of America* **2015,** *112* (35), 10857-10862.

14.   Qiu, J.; Tonokura, K., Detection of the simplest Criegee intermediate CH_2OO in the v4 band using a continuous wave quantum cascade laser and its kinetics with SO_2 and NO_2. *Chem. Phys. Lett.: X* **2019,** *2*, 100019.

15.   Liu, Y. D.; Bayes, K. D.; Sander, S. P., Measuring Rate Constants for Reactions of the Simplest Criegee Intermediate (CH2OO) by Monitoring the OH Radical. *Journal of Physical Chemistry A* **2014,** *118* (4), 741-747.

16.   Liu, Y. Q.; Liu, F. H.; Liu, S. Y.; Dai, D. X.; Dong, W. R.; Yang, X. M., A kinetic study of the CH_2OO Criegee intermediate reaction with SO_2, (H_2O)2, CH_2I_2 and I atoms using OH laser induced fluorescence. *Physical Chemistry Chemical Physics* **2017,** *19* (31), 20786-20794.

17.   Cox, R. A.; Ammann, M.; Crowley, J. N.; Herrmann, H.; Jenkin, M. E.; McNeill, V. F.; Mellouki, A.; Troe, J.; Wallington, T. J., Evaluated kinetic and photochemical data for atmospheric chemistry: Volume VII - Criegee intermediates. *Atmos. Chem. Phys.* **2020,** *20* (21), 13497-13519.

Physical Chemistry Chemical Physics Accepted Manuscript

18.   Taatjes, C. A.; Welz, O.; Eskola, A. J.; Savee, J. D.; Scheer, A. M.; Shallcross, D. E.; Rotavera, B.; Lee, E. P. F.; Dyke, J. M.; Mok, D. K. W.; Osborn, D. L.; Percival, C. J., Direct Measurements of Conformer-Dependent Reactivity of the Criegee Intermediate CH_3CHOO. *Science* **2013,** *340* (6129), 177-180.

19.   Wang, Y. Y.; Dash, M. R.; Chung, C. Y.; Lee, Y. P., Detection of transient infrared absorption of SO_3 and 1,3,2-dioxathietane-2,2-dioxide cyc-$(CH_2)O(SO_2)O$ in the reaction CH_2OO+SO_2. *Journal of Chemical Physics* **2018,** *148* (6).

20.   Jiang, L.; Xu, Y. S.; Ding, A. Z., Reaction of Stabilized Criegee Intermediates from Ozonolysis of Limonene with Sulfur Dioxide Ab Initio and DFT Study. *Journal of Physical Chemistry A* **2010,** *114* (47), 12452-12461.

21.   Kurtén, T.; Lane, J. R.; Jorgensen, S.; Kjaergaard, H. G., A Computational Study of the Oxidation of SO_2 to SO_3 by Gas-Phase Organic Oxidants. *Journal of Physical Chemistry A* **2011,** *115* (31), 8669-8681.

22.   Kuwata, K. T.; Guinn, E. J.; Hermes, M. R.; Fernandez, J. A.; Mathison, J. M.; Huang, K., A Computational Re-examination of the Criegee Intermediate-Sulfur Dioxide Reaction. *Journal of Physical Chemistry A* **2015,** *119* (41), 10316-10335.

23.   Aplincourt, P.; Ruiz-López, M. F., Theoretical investigation of reaction mechanisms for carboxylic acid formation in the atmosphere. *Journal of the American Chemical Society* **2000,** *122* (37), 8990-8997.

24.   Novelli, A.; Hens, K.; Ernest, C. T.; Martinez, M.; Nolscher, A. C.; Sinha, V.; Paasonen, P.; Petaja, T.; Sipila, M.; Elste, T.; Plass-Dulmer, C.; Phillips, G. J.; Kubistin, D.; Williams, J.; Vereecken, L.; Lelieveld, J.; Harder, H., Estimating the atmospheric concentration of Criegee intermediates and their possible interference in a FAGE-LIF instrument. *Atmospheric Chemistry and Physics* **2017,** *17* (12), 7807-7826.

25.   Pierce, J. R.; Evans, M. J.; Scott, C. E.; D'Andrea, S. D.; Farmer, D. K.; Swietlicki, E.; Spracklen, D. V., Weak global sensitivity of cloud condensation nuclei and the aerosol indirect effect to Criegee + SO_2 chemistry. *Atmospheric Chemistry and Physics* **2013,** *13* (6), 3163-3176.

26.   Chao, W.; Hsieh, J. T.; Chang, C. H.; Lin, J. J. M., Direct kinetic measurement of the reaction of the simplest Criegee intermediate with water vapor. *Science* **2015,** *347* (6223), 751-754.

27.   Lewis, T. R.; Blitz, M. A.; Heard, D. E.; Seakins, P. W., Direct evidence for a substantive reaction between the Criegee intermediate, CH_2OO, and the water vapour dimer. *Physical Chemistry Chemical Physics* **2015,** *17* (7), 4859-4863.

28.   Smith, M. C.; Chang, C. H.; Chao, W.; Lin, L. C.; Takahashi, K.; Boering, K. A.; Lin, J. J. M., Strong Negative Temperature Dependence of the Simplest Criegee Intermediate CH_2OO Reaction with Water Dimer. *J. Phys. Chem. Lett.* **2015,** *6* (14), 2708-2713.

29.   Lin, L. C.; Chang, H. T.; Chang, C. H.; Chao, W.; Smith, M. C.; Chang, C. H.; Lin, J. J. M.; Takahashi, K., Competition between H_2O and $(H_2O)_2$ reactions with CH_2OO/CH_3CHOO. *Physical Chemistry Chemical Physics* **2016,** *18* (6), 4557-4568.

30.   IUPAC Task Group on Atmospheric Chemical Kinetic Data Evaluation, http://iupac.pole-ether.fr. (accessed 18.06.2021).

31.   Lewis, T.; Heard, D. E.; Blitz, M. A., A novel multiplex absorption spectrometer for time-resolved studies. *Review of Scientific Instruments* **2018,** *89* (2).

32.   Mir, Z. S.; Lewis, T. R.; Onel, L.; Blitz, M. A.; Seakins, P. W.; Stone, D., CH_2OO Criegee intermediate UV absorption cross-sections and kinetics of $CH_2OO + CH_2OO$ and $CH_2OO + I$ as a function of pressure. *Physical Chemistry Chemical Physics* **2020,** *22* (17), 9448-9459.

33.   Onel, L.; Blitz, M.; Seakins, P.; Heard, D.; Stone, D., Kinetics of the Gas Phase Reactions of the Criegee Intermediate CH_2OO with O_3 and IO. *J. Phys. Chem. A* **2020,** *124* (31), 6287-6293.

34.   Spietz, P.; Martin, J. C. G.; Burrows, J. P., Spectroscopic studies of the I_2/O_3 photochemistry - Part 2. Improved spectra of iodine oxides and analysis of the IO absorption spectrum. *Journal of Photochemistry and Photobiology a-Chemistry* **2005,** *176* (1-3), 50-67.

35.   Burkholder, J. B., Sander, S. P., Abbatt, J. P. D., Barker, J. R., Huie, R. E., Kolb, C. E., Kurylo, M. J., Orkin, V. L., Wilmouth, D. M., Wine, P. H., Chemical kinetics and photochemical data for use in atmospheric studies - Evaluation No. 18. JPL Publication 15-10: available at: http://jpldataeval.jpl.nasa.gov/, last access: 25 May 2021, 2015.

36.   Stone, D.; Blitz, M.; Daubney, L.; Ingham, T.; Seakins, P., CH_2OO Criegee biradical yields following photolysis of CH_2I_2 in O_2. *Phys. Chem. Chem. Phys.* **2013,** *15* (44), 19119-19124.

37.   https://mathworld.wolfram.com/Erf.html. (accessed 18.06.2021).

38.   Glowacki, D. R.; Liang, C. H.; Morley, C.; Pilling, M. J.; Robertson, S. H., MESMER: An Open-Source Master Equation Solver for Multi-Energy Well Reactions. *Journal of Physical Chemistry A* **2012,** *116* (38), 9545-9560.

39.   Shannon, R. J.; Caravan, R. L.; Blitz, M. A.; Heard, D. E., A combined experimental and theoretical study of reactions between the hydroxyl radical and oxygenated hydrocarbons relevant to astrochemical environments. *Phys. Chem. Chem. Phys.* **2014,** *16* (8), 3466-3478.

Physical Chemistry Chemical Physics Accepted Manuscript

40.   Stone, D.; Au, K.; Sime, S.; Medeiros, D. J.; Blitz, M.; Seakins, P. W.; Decker, Z.; Sheps, L., Unimolecular decomposition kinetics of the stabilised Criegee intermediates CH$_2$OO and CD$_2$OO. *Phys. Chem. Chem. Phys.* **2018,** *20* (38), 24940-24954.

41.   Whelan, C. A.; Blitz, M. A.; Shannon, R.; Onel, L.; Lockhart, J. P.; Seakins, P. W.; Stone, D., Temperature and Pressure Dependent Kinetics of QOOH Decomposition and Reaction with O2: Experimental and Theoretical Investigations of QOOH Radicals Derived from Cl + (CH$_3$)$_3$COOH. *J. Phys. Chem. A* **2019,** *123* (47), 10254-10262.

42.   Medeiros, D. J.; Blitz, M. A.; James, L.; Speak, T. H.; Seakins, P. W., Kinetics of the Reaction of OH with Isoprene over a Wide Range of Temperature and Pressure Including Direct Observation of Equilibrium with the OH Adducts. *J. Phys. Chem. A* **2018,** *122* (37), 7239-7255.

43.   Lynch, B. J.; Truhlar, D. G., Robust and affordable multicoefficient methods for thermochemistry and thermochemical kinetics: The MCCM/3 suite and SAC/3. *J. Phys. Chem. A* **2003,** *107* (19), 3898-3906.

44.   Smith, M. C.; Chao, W.; Takahashi, K.; Boering, K. A.; Lin, J. J. M., Unimolecular Decomposition Rate of the Criegee Intermediate (CH$_3$)$_2$COO Measured Directly with UV Absorption Spectroscopy. *Journal of Physical Chemistry A* **2016,** *120* (27), 4789-4798.

45.   NIST/SEMATECH   e-Handbook   of   Statistical   Methods. http://www.itl.nist.gov/div898/handbook/ (accessed 18.05.2021).

46.   Ruscic, B., Active Thermochemical Tables: Water and Water Dimer. *J. Phys. Chem. A* **2013,** *117* (46), 11940-11953.